ACOUSTICS 2017 PERTH
SOUND, SCIENCE AND SOCIETY

Quantitative analysis on the environmental impact benefits from the bandwidth-controlled marine seismic source technology

Binghui Li (1) and Martin Bayly (2)

(1) SLR Consulting Australia Pty Ltd, Ground Floor, 503 Murray Street, Perth, 6000, Western Australia
(2) WesternGeco, Level 5, 256 St Georges Terrace, Perth, WA 6000, Western Australia

ABSTRACT

A new marine seismic surveying source technology (*eSource*) has recently been developed based on physical control of the bandwidth of the source elements (Coste et al., 2014). The objective of the new seismic source is to reduce the potential environmental impact of seismic surveying operations on marine life. This new seismic source greatly limits the energy emissions at higher frequencies, while retaining the low-frequency bandwidth output that is crucial to seismic survey imaging.

This paper firstly introduces the new seismic source design considerations based on a literature review, followed by the eSource signature outputs simulated using the commercial airgun source modelling software package Gundalf™. In comparison with the conventional seismic sources, the potential environmental impact benefits from the new source are analysed in detail under different frequency weighting systems proposed for low-frequency (LF), mid-frequency (MF) and high-frequency (HF) hearing cetacean groups. This quantitative analysis is supplemented with a case study of an array arrangement comprising of conventional/eSource array elements that has been modelled and subsequently implemented for a marine seismic survey within the North West Shelf of Western Australia.

1 INTRODUCTION

Underwater airgun devices are the most widely used sound sources for marine geophysical surveying since the 1960s (Parks and Hatton, 1986). These devices typically consist of air chambers filled with high-pressure air which, when being rapidly released, generate acoustic pulses as a result of the initial expulsion of air and the subsequent expansion and contraction of the air bubble released from the chamber. Normally an arrangement of multiple airgun devices in a planar array is used to improve the source performance via amplification of the primary pulse and partial cancellation of subsequent oscillating bubbles (Ziolkowski, 1970).

The frequency content of interest from the sound sources for the sub-surface geophysical imaging purposes is typically below 100 Hz (Gisiner, 2016). The high frequency energy components emitted by the source elements are not useful from a geophysical imaging perspective and are generally immediately rejected by the high cut filters (the cut-off frequency typically around 200 Hz) within the acquisition and digitization system. However, this high-frequency energy component from the sound sources is still emitted into the marine environment. This energy may pose a potential environmental risk for marine life within or near the area of operations. Modelling and understanding the emitted energy levels of a potential seismic survey is a requirement for obtaining an environmental permit to operate in many jurisdictions. As such, preserving the useful low-frequency energy component while limiting the high frequency energy emissions from the sound sources is a desirable and balanced objective for any alternative geophysical sound source.

To achieve this objective, WesternGeco, Schlumberger and Teledyne Bolt Technology Corporation have jointly developed a new type of seismic source, i.e. “eSource”, based on bandwidth-controlled marine seismic source technology (Coste et al, 2014). Coste et al (2014) analysed the near-field measurements for a standard airgun pulse, and concluded that the high-frequency energy component of airgun acoustic emissions primarily comes from the steep rising edge of the primary pulse, when the high-pressure air is initially released from the airgun portal. The control of the steepness of the rising edge of the primary pulse has been modelled and understood based on 3D computational fluid dynamics (CFD) simulation of the air release and flow mechanisms during the pulse onset. This has led to a physical redesign of both the exit ports and internal air releasing valve (Coste et al, 2014, Gerez et al, 2015, Teledyne Blog, 2017).

The eSource type airguns have been manufactured and tested by Teledyne Bolt Technology Corporation (2017). Figure 1 shows the comparison between the conventional Bolt 1900 LLXT airgun with rectangular port

shape and the eSource Bolt 500A airgun with a “tear drop” port shape that is crucial for controlling the pulse onset.

Figure 1: The conventional Bolt 1900 LLXT airgun with rectangular port shape (left) and the eSource Bolt 500A (right) airgun with the unusual port shape (Ref: http://www.teledynemarine.com/air-guns/).

2 SOURCE SIGNATURE MODELLING

2.1 Gundalf: Marine Seismic Airgun Modelling Software Package

As one of the commercial marine seismic airgun modelling software package, Gundalf™ (2016) is claimed to have been rigorously calibrated against large datasets of signatures of various gun types recorded in specialist facilities, including the various eSource gun types currently available.

The signature outputs of either single airgun units or airgun arrays presented in this paper were simulated using Gundalf Designer software package.

2.2 The single 100 CUI conventional 1900LLX and eSource 500A

Taking a single gun unit of 100 cubic inch (CUI) situated at a depth of 6 m below the sea surface as an example, the comparisons between the conventional Bolt 1900LLX and eSource 500A in both signature waveforms and the power spectral densities (PSDs) are illustrated in Figure 2. As can be seen from inset zoon image of the initial sections of the signature waveforms in the figure, the conventional Bolt gun unit produces much steeper rising edge of the primary pulse than the eSource gun unit. This leads to higher PSD level of acoustic energy emitted from the conventional Bolt gun unit than from the eSource gun for frequencies approximately above 120 Hz. The difference between the two PDSs generally increases with frequency and can be up to 30 dB for frequencies approximately above 600 Hz.

It should be noted that this comparison uses the eSource “A” configuration (Gerez 2014) which is the mildest option for higher frequency attenuation, other eSource options (‘B” and “C”) are more aggressive.

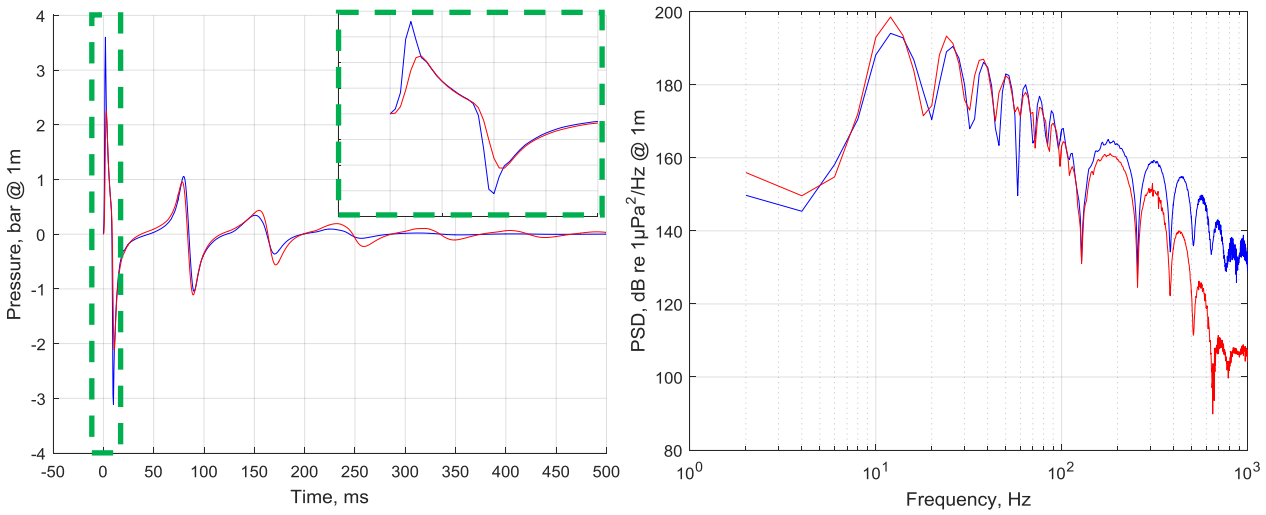

Figure 2: The conventional Bolt 1900 LLX (blue) and the eSource 500A (red) airgun signatures with the surface ghost of 6-m water depth (left panel), and their corresponding PSDs (right panel) for a single gun unit of 100 CUI. The first 15 ms (zoom display) of the initial primary pulse is inserted (green dash frame).

2.3 The conventional/eSource 3,147 CUI airgun array

The comparisons in both signature waveforms and the PSDs are also carried out for an airgun array of 3,147 CUI comprising of either conventional or eSource airgun units. The configuration of the 3,147 CUI array is shown in Figure 3. The array comprises three subarrays, and each subarray has eight source elements, arranged as single sources or in clusters. For the conventional array, the gun types for the 24 elements of the array are either 1900LLX (Vol > 100 CUI) or 1500LL (Vol <100 CUI), and for the eSource array, the gun types are either e500A (Vol > 100 CUI) or e300A (Vol <100 CUI). Essentially the two arrays being compared are the same apart from the use of the e-Source type elements rather than conventional. The array has an average towing depth of 7.5 m and an operating pressure of 2,000 pounds per square inch (PSI). This is a standard WesternGeco "Delta-3" array configuration.

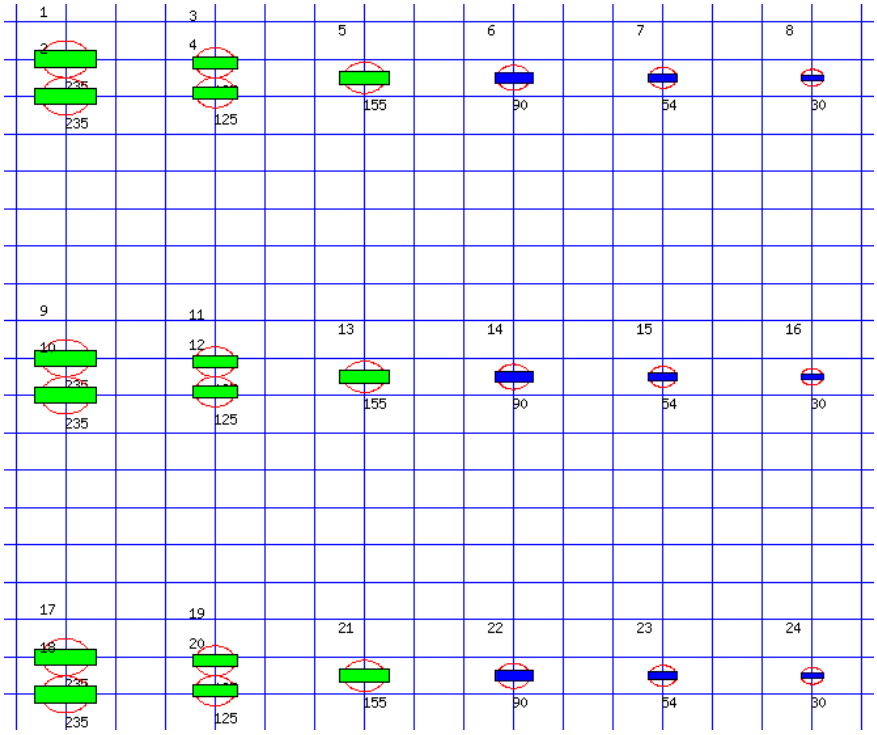

Figure 3: The configuration (numbers above/below the guns are their sequential numbers/volumes) of the conventional (/eSource) 3,147 CUI airgun array in a 1m-grid plan view. Gun types are either 1900LLX (/e500A) (green) or 1500LL (/e300A) (blue) airguns. The in-line direction for the source array is the east-west direction.

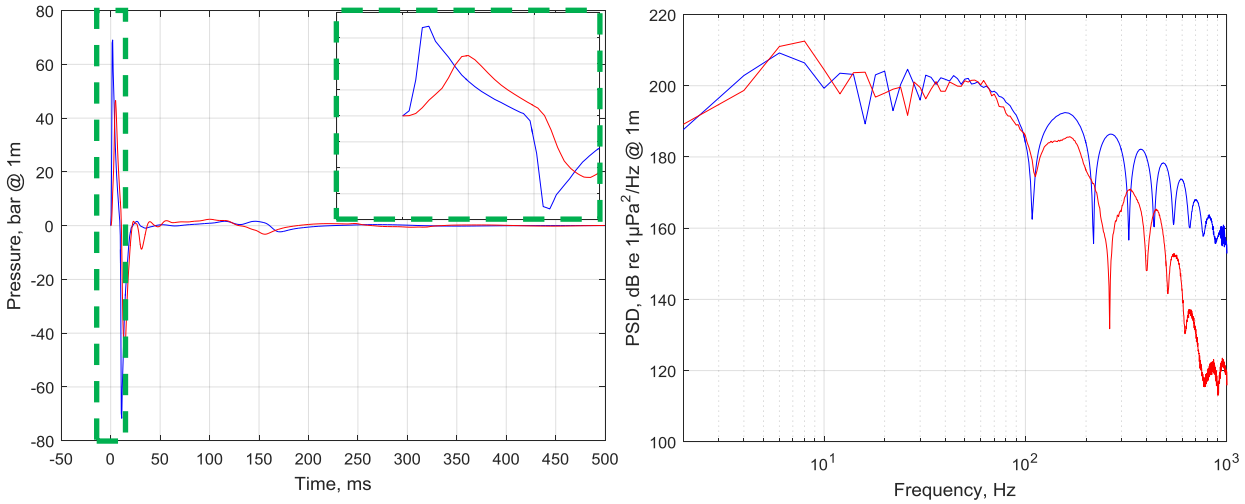

Figure 4: The far-field signatures (left panel) in vertically downward direction and the corresponding PSDs (right panel) for the conventional (blue) and the eSource "A" (red) 3147 CUI arrays. The first 15 ms (zoom display) of the initial primary pulse is inserted (green dash frame).

Figure 4 presents the simulated far-field signatures of the arrays with both conventional and eSource airguns and their corresponding PSDs. Compared with the source signature of single airgun unit as shown in Figure 2, the distinctive characteristics of the far-field signatures of the source array are the significantly suppressed bubble oscillations following the primary pulses in signature waveforms, and relatively less variability in the PSDs at the low frequencies below 100 Hz. Compared to the single airgun case, the difference in steepness of the rising edge of the primary pulse between the conventional and eSource array source signatures is higher. As a result, the differences between the PDSs of conventional and eSource airgun arrays are greater than the single airgun case, and can be up to 40 dB for some frequencies above 700 Hz.

The beam patterns in PSD in the horizontal plane for both conventional and the eSource A source arrays, as a function of azimuth angle and frequency, are presented in Figure 5. These beam patterns illustrate the strong angle and frequency dependence of the energy radiation from the array, with relatively higher energy radiation in the cross-line direction than in the in-line direction. The predominant frequency variation characteristics of these beam patterns are a result of interference between signals from different array elements, particularly from the three sub-array elements. The beam pattern from the eSource array demonstrates significantly lower energy radiations than the conventional array for frequencies approximately above 600 Hz in all directions.

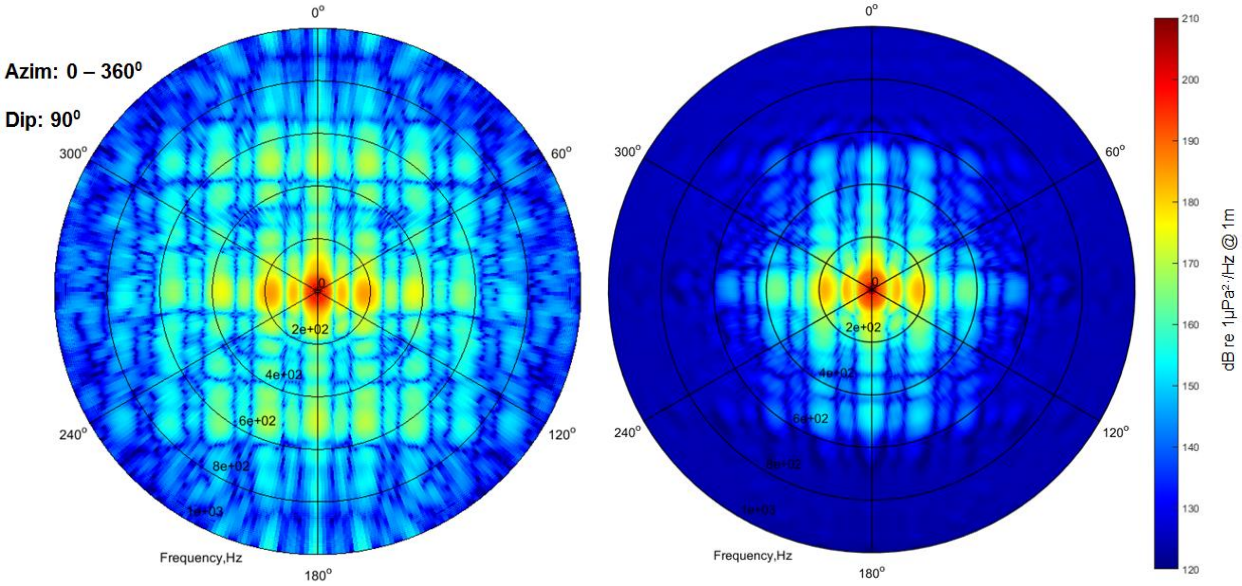

Figure 5: Array far-field beam patterns of PSD in the horizontal plane (Dip angle 90^0) for the conventional (left panel) and the eSource (right panel) 3,147 CUI array, as a function of orientation (Azimuth 0^0 – 360^0) and frequency (1 – 1000Hz). Azimuth 0^0 corresponds to the in-line direction of the source array.

3 ENVIRONMENTAL BENEFITS UNDER DIFFERENT FREQUENCY WEIGHTING SYSTEMS

3.1 Frequency weighting systems

Marine mammals have different hearing sensitivities towards different sound frequencies, and tend to be increasingly less sensitive towards both the low and high end of their hearing ranges, which is generally reflected in the common U-shape of audiograms (Au and Hastings, 2008).

There are a few different frequency weighting systems that have been proposed for cetacean species, with each weighting system consisting of separate weighting functions for different hearing groups (i.e. low-frequency (LF), mid-frequency (MF) and high-frequency (HF)) of cetaceans. Southall et al. (2007) proposed that frequencies to be weighted with a fairly broad weighting function (i.e. M-weighting) which only removes very low and very high frequencies that are well outside the range of best hearing for the animals. National Marine Fisheries Service (NMFS) (2016) introduced a more restrictive weighting system with the weighting filter functions resembling the inversed audiograms. The U.S. Navy (Finneran and Schlundt, 2013) developed an intermediate form weight system (Type II Navy weighting functions) utilising features of both the M-weighting functions and the equal loudness (EQL) weighting functions.

The three plots in Figure 6 present these three different frequency weighting systems (i.e. M, Audiogram and Type II Navy) for LF, MF and HF hearing group of cetaceans respectively. In comparison, the Audiogram-weighting system in general is the most conservative weighting system among the three in terms of hearing sensitivity, particularly for the MF and HF cetacean groups, while the M-weighting system reflects the most sensitivities hearing abilities for the three hearing groups of cetaceans.

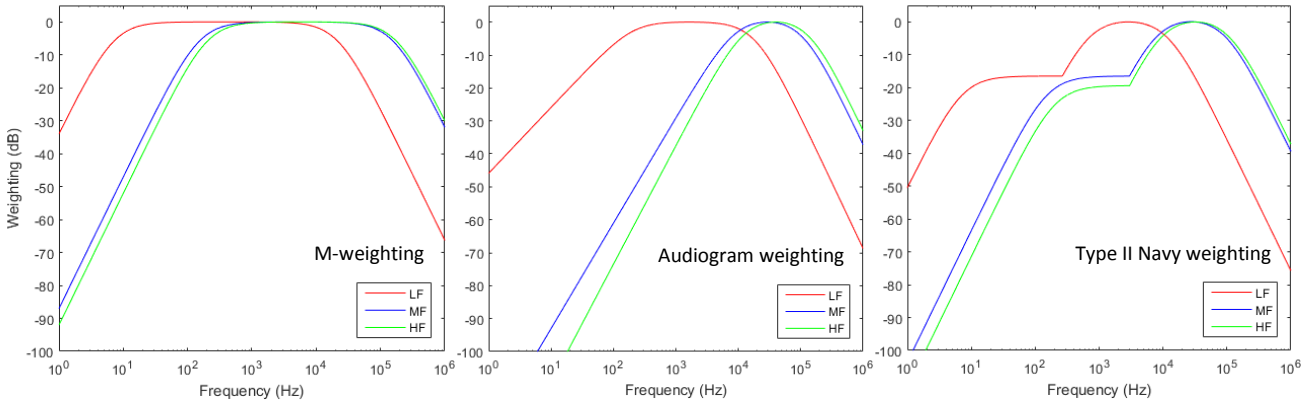

Figure 6: Three frequency weighting systems (M-weighting (left panel), Audiogram weighting (middle panel) and Type II Navy weighting (right panel)) for the LF, MF and HF cetacean group.

3.2 Weighted Far-field Source Signature PSDs and Sound Exposure Levels (SELs) – Conventional vs eSource "A" 3147 CUI array

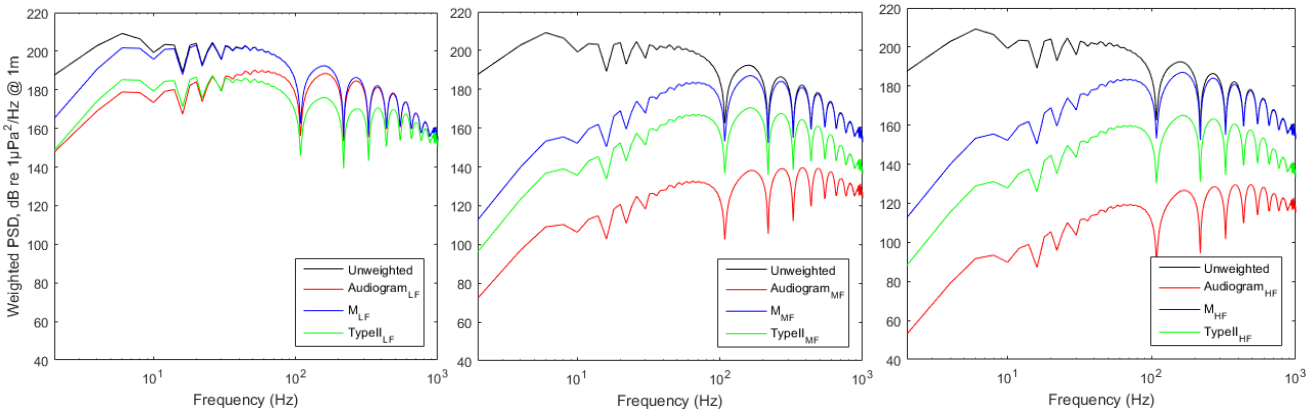

Figure 7: The source PSDs of the conventional Bolt 3147 CUI array with different frequency weighting systems (i.e. unweighted, M, Audiogram and Type II Navy) for the LF (left), MF (middle) and HF (right) cetacean group.

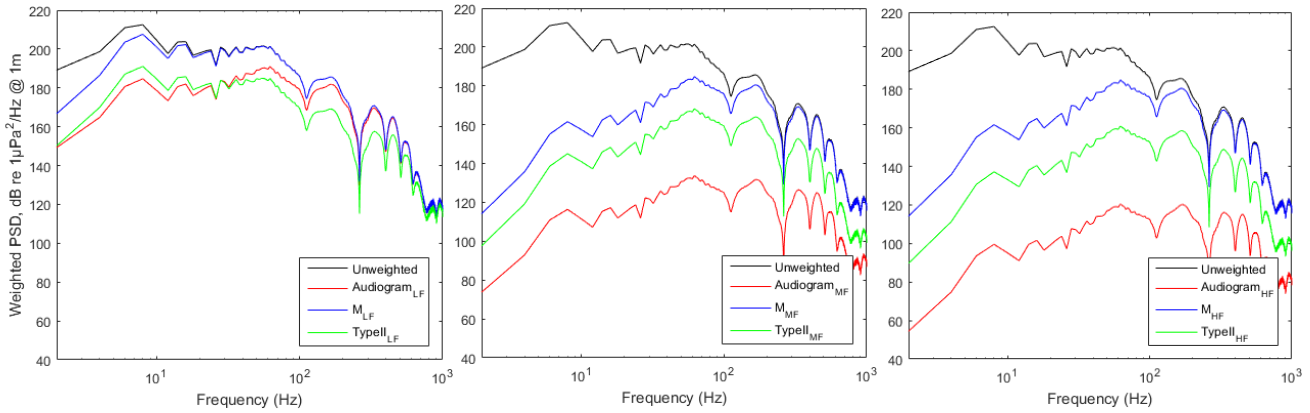

Figure 8: The source PSDs of the eSource Bolt 3147 CUI array with different frequency weighting systems (i.e. unweighted, M, Audiogram and Type II Navy) for the LF (left), MF (middle) and HF (right) cetacean group.

The weighted far-field (directly downward) source signature PSDs of the conventional Bolt 3147 CUI source array for the three (i.e. LF, MF and HF) hearing cetacean groups under four weighting systems (i.e. Unweighted,

Audiogram, M and Type II Navy) are presented in Figure 7, and of the eSource 3147 CUI array in Figure 8. It should be noted that only initial sections (i.e. 0 – 1 kHz in frequency) of the weighting functions in Figure 6 are applicable for the weighted PSD calculations, due to the same frequency limit in PSDs.

For each frequency weighting system, in line with the discrepancies in frequency weighing functions for different hearing groups as presented in Figure 6, weighted PSDs for the LF hearing group have the lowest discrepancies from the unweighted PSD, while the discrepancies are the highest for the HF hearing group. In general, the discrepancies between the unweighted and weighted PSDs tend to increase with decreasing frequency.

Among the three frequency weighting systems, the weighted PSDs under the M-weighting system remain as the highest for all three hearing groups. The weighted PSDs under the audiogram weighting system have the lowest PSD curves across the frequency range for MF and HF hearing groups, while for LF hearing group the PSD curve under the Type II Navy weighting being the lowest for frequencies above 30 Hz.

For both conventional and eSource 3,147 CUI airgun array, the overall source SELs for the three hearing functions under different frequency weighting systems are summarised in Table 1. The overall SELs are generally in reflection with the discrepancies in weighted PSDs as described above, and as clearly being demonstrated, the HF hearing group benefits the most from the eSource source array arrangement under the audiogram weighting system.

Table 1: Overall source SELs for both conventional and eSource 3,147 CUI airgun array under different frequency weighting systems.

Frequency Weighting System	Source SEL, *dB re 1μPa^2·S @ 1 m*					
	LF Hearing Function		MF Hearing Function		HF Hearing Function	
	Conventional	eSource	Conventional	eSource	Conventional	eSource
Unweighted	224.2	224.4	224.2	224.4	224.2	224.4
M	222.9	222.1	210.8	204.5	208.7	201.1
Type II Navy	206.7	205.6	194.3	188.0	189.2	181.7
Audiogram	213.4	209.6	167.0	155.6	156.9	143.9

4 A CASE STUDY – SEISMIC SURVEY IN NORTH WEST SHELF, WESTERN AUSTRALIA

In early 2016 WesternGeco has proposed to undertake an offshore seismic survey in the North West Shelf (NWS) area of Western Australia. SLR Consulting Australia Pty Ltd (SLR) was engaged by WesternGeco to undertake a sound transmission loss modelling study as part of the environmental permitting process. Subsequently the survey was acquired in late 2016 to early 2017 using eSource components (Bayly et al., 2017). The pre-survey sound study was important as the survey is adjacent ecologically sensitive areas. This modelling exercise investigated the two array source options, i.e. the conventional and the eSource “A” 3,147 CUI airgun arrays as described in Section 2.3, and the differences in the sound fields resulting from the two source arrays at differing ranges from the array source location.

4.1 Sound speed profile

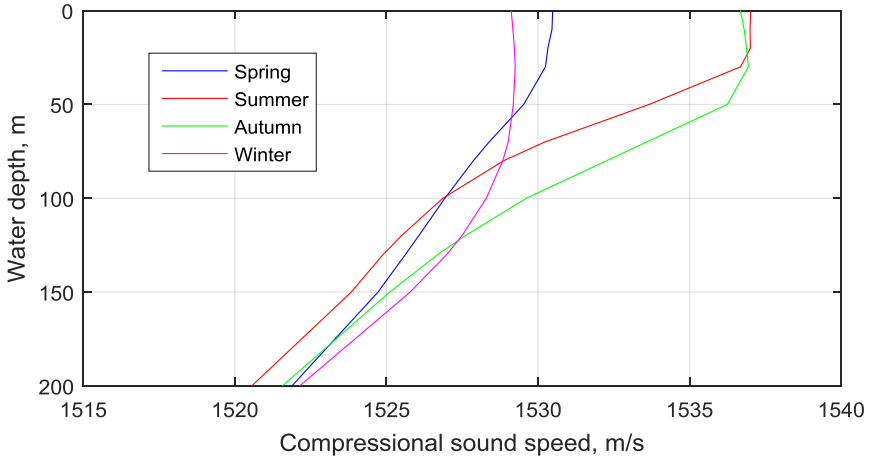

Figure 9: Typical sound speed profiles within close proximity to the survey area off the coast of North West Australia for different southern hemisphere seasons.

The sections below present a modelling case within a shallow water environment (depth of 31 m) for a near-field (out to 4,000 metres range) sound field scenario, with consideration of interference effects between the arriving signals from different source elements in the source array.

The temperature and salinity data required to derive the sound speed profiles were obtained from the World Ocean Atlas 2009 (WOA09) (Locarnini et al., 2010; Antonov et al., 2010). The hydrostatic pressure needed for calculation of the sound speed based on depth and latitude of each particular sample was obtained using Sanders and Fofonoff's formula (Sanders and Fofonoff, 1976). The sound speed profiles were derived based on Del Grosso's equation (Del Grosso, 1974).

Figure 9 above shows typical seasonal sound speed profiles in the survey area off the coast of North West Australia. The most significant seasonal differences in speed profiles occur within the mixed layer near the sea surface. The depth of the mixed surface layer varies with the seasons, and is deeper in the winter than in other seasons. The seasonal speed profiles indicate that the winter season is expected to be most favourable to propagation of sound from the near-surface source array. For this case the survey was undertaken in summer season, and therefore the summer season sound speed profile was used for the modelling case study.

4.2 Seafloor geo-acoustic model

The seafloor over a large part of Australia's continental shelf, particularly the southern and western areas, consists of a particular type of limestone called calcarenite. This calcarenite layer is overlain by a thin (up to 1.0 m) veneer of unconsolidated sediment (Duncan et al., 2009).

Table 2: Geoacoustic properties for silt-sand sediment and calcarenite substrate.

Seafloor Layers and Materials	Density, ρ, $(kg.m^{-3})$	Compressional Wave		Shear Wave	
		Speed, c_p, $(m.s^{-1})$	attenuation, α_p, (dB/λ)	Speed, c_s, $(m.s^{-1})$	attenuation, α_s, (dB/λ)
Top Layer - silt-sand (fluid)	1800	1600	0.9	-	-
Substrate - calcarenite (elastic)	2400	2800	0.1	1400	0.2

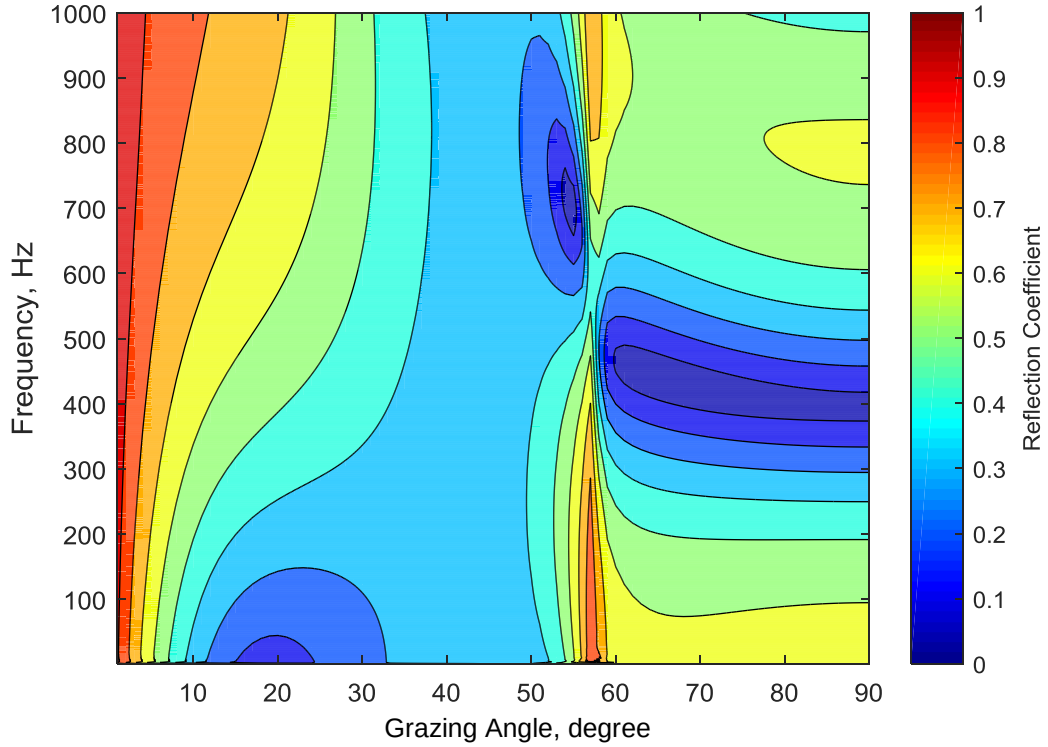

Figure 10: Reflection coefficient variations with grazing angle and frequency for the geoacoustic model given in Table 2.

The geoacoustic properties of the typical silt-sand fluid top sediment and the elastic calcarenite seafloor substrate material are outlined in Table 2, based on database from the literature (Hamilton, 1980 and Jensen et al., 2000). The corresponding reflection coefficient variations with grazing angle and frequency calculated based on Bounce algorithm (Porter, 2010) are presented in Figure 10, noting that the high reflection coefficients at high frequencies and high grazing angles is due to the elastic characteristics of the calcarenite (Duncan et al., 2009, Li and Hall, 2012).

4.3 Modelling methodology and procedure

For receiving locations within a few kilometres to the source array, interference effects between the signals arriving at any receiving location from different source elements in the source array are expected to be significant and complex for such near-field scenario. To account for these considerations, the near-field case predictions are modelled by reconstructing and adding the received signal waveforms from individual source array units.

The wavenumber integration modelling algorithm SCOOTER (Porter, 2010) is used to calculate the transfer functions (both amplitudes and phases) between sources and receivers. SCOOTER is a finite element code for computing acoustic fields in range-independent environments. The method is based on direct computation of the spectral integral, and is capable of dealing with an arbitrary layered seabed with both fluid and elastic characteristics.

The following procedures have been followed to calculate received SELs for the near-field modelling scenario:

1) The modelling algorithm SCOOTER is executed for frequencies from 1 Hz to 1 kHz, in 1 Hz increments. The source depth is taken to be the average source array depth of 7.5 m. A 1 m receiver grid in both range and depth with a maximum range up to 4.0 km is applied for the selected water depth. For each 1 m gridded receiver, the received SEL is calculated by following steps 2) – 5);
2) The range from each source in the array to each receiver is calculated, and the transfer function between each source and the receiver is obtained by interpolation of the results produced by modelling algorithm SCOOTER in Step 1). This interpolation involves both amplitude and phase of the signal waveform in frequency domain;
3) The complex frequency domain signal of the notional signature waveform for each source is calculated via Fourier Transform, and multiplied by the corresponding transfer function from Step 2) to obtain the frequency domain representation of the received signal from that particular source element;
4) The waveform of received signal from each source is reconstructed via Inverse Fourier Transform. The received signal waveforms from all source elements in the array are summed to obtain the overall received signal waveform; and
5) The overall signal waveform is squared and integrated over time to obtain the received SEL value. Alternatively, the SEL value can also be calculated via integration of the energy power density (ESD) over frequency in Step 3).

4.4 Modelling results

The modelling results indicate that the highest SEL levels occur in the in-line and cross-line directions, as a result of the directionality of the source array geometry. Figure 11 below presents the predicted near-field sound fields in SEL (dB re 1μPa^2·s) over a cross section in the cross-line direction as a function of water depth (0 – 31m) and range (0 – 4km) from the centre of the source array for both conventional and eSource 3,147 CUI airgun array. It is noticeable that for this particular cross section the sound field from the eSource source array has higher attenuation with range in comparison to the sound field from the conventional source array.

A scatter plot of the predicted maximum SELs across the water column for all azimuths is displayed in Figure 12 as a function of range from the centre of the source, for both conventional and eSource 3,147 CUI airgun array. The predictions of the maximum SELs received at various ranges from the centre of the array are also listed in Table 2 for the two source arrays.

As can be seen from Figure 12 and Table 2, the predicted SELs from the two source arrays have similar values (within 1dB difference) within 100 m of the array. This is due to the fact that the low frequency energy dominates the noise emissions for the two source arrays. As the distance increases, the SELs from the eSource source array are noticeably lower than from the conventional source array (e.g. 4.2 dB in difference at 1.0km and 5.3 dB at 2.0 km), and the differences increase further with distance. This is due to the higher attenuation for low frequency energy component over the modelling range within such a shallow water environment, as well as the significantly lower energy emissions at higher frequencies from the eSource source array, as being evidently shown in Figure 4 and Figure 5.

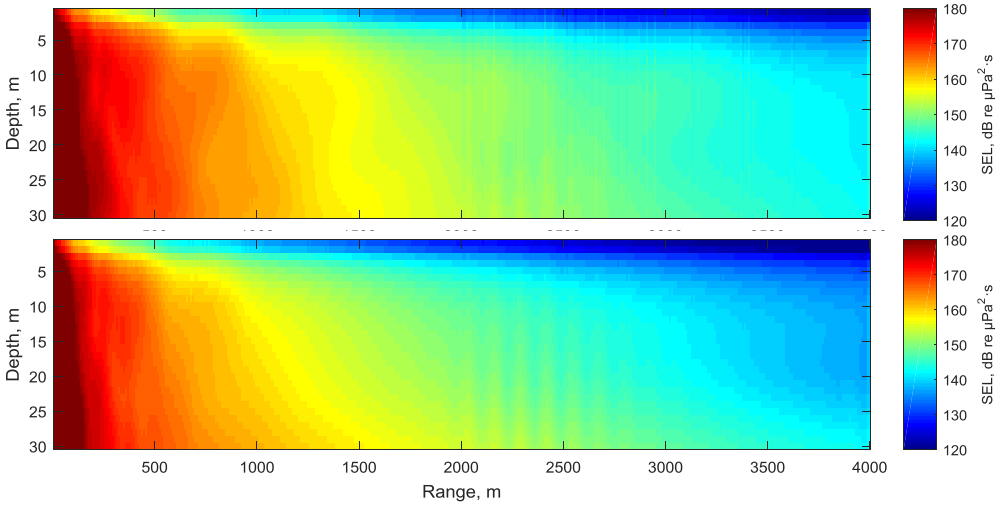

Figure 11: The predicted SELs along the cross-line direction as a function of water depth (0 – 31m) and range (0 – 4km) from the centre of the array for both conventional (top) and eSource (bottom) 3,147 CUI airgun array.

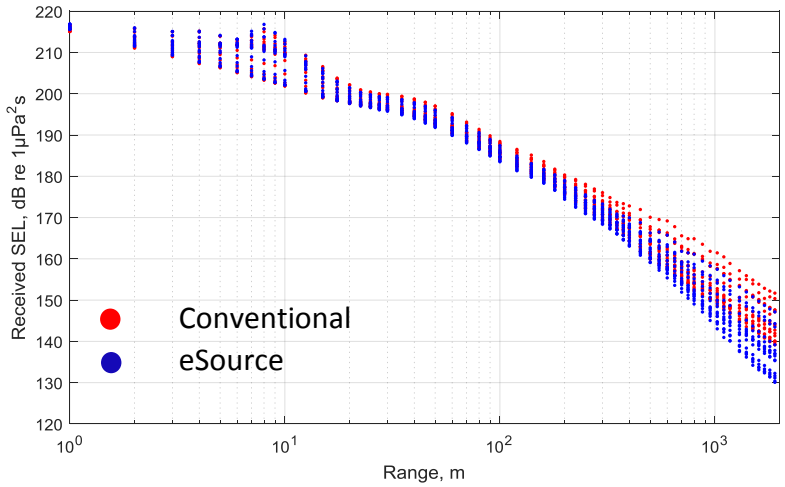

Figure 12: Predicted maximum SELs as a function of range from the center of the source array across the water columns and over all azimuths for both conventional (red) and eSource (blue) 3,147 CUI airgun array.

Table 3: Predicted maximum SEL for all azimuths at various ranges from the center of the source array for both conventional and eSource 3,147 CUI airgun array.

Source Array Configuration	Maximum SEL at different *ranges, dB re 1μPa²·s*							
	10 m	50 m	100 m	200 m	500 m	1.0 km	1.5 km	2.0 km
Conventional	213.0	198.2	188.4	180.3	170.5	162.5	155.6	152.5
eSource	213.0	196.1	187.4	179.0	168.1	158.3	151.2	147.2

5 CONCLUSIONS

This paper demonstrates a detailed modelling investigation and quantitative analysis on the sound emitted into the environment and potential environmental impact benefits from the newly introduced bandwidth-controlled marine seismic source (*eSource*), when compared with a similar size conventional seismic source array. This paper demonstrates that the eSource technology has great application in reducing potential harm for marine mammals especially when evaluated when using the weighting schemes such as the MF and HF cetacean groups and particularly under the audiogram-weighting system. In addition even without weighting, the eSource has a significant emission reduction at horizontal ranges exceeding 1000m in shallow water that is often environmentally sensitive. In both cases this is due to the eSource technology significantly suppressing the energy emissions at high frequencies that are not required for sub surface seismic surveying.

6 ACKNOWLEDGEMENT

The authors would like to acknowledge WesternGeco and SLR for permission to publish this work.

REFERENCES

Antonov JI, Seidov D, Boyer TP, Locarnini RA, Mishonov AV, Garcia HE, Baranova OK, Zweng MM, and Johnson DR, 2010, World Ocean Atlas 2009, Volume 2: Salinity. S. Levitus, Ed. NOAA Atlas NESDIS 69, U.S. Government Printing Office, Washington, D.C., 184 pp.

Au WWL and Hastings MC, 2008, Principles of Marine Bioacoustics. New York: Springer-Verlag.

Bayly M, Tham M, Waterson P, Li B and Moran K, 2017, Marine seismic acquisition: efficiency & environment, new technologies applied in Australia, The APPEA Journal 57(2) 704-708 https://doi.org/10.1071/AJ16072.

Coste E, Gerez D, Groenaas H, Hopperstad JF, Larsen OP, Laws R, Norton J, Padula M and Wolfstirn M, 2014, Attenuated high-frequency emission from a new design of airgun, 84th Annual International Meeting, SEG, Expanded Abstracts, 132–137.

Del Grosso VA, 1974, New equation for the speed of sound in natural waters (with comparisons to other equations), J. Acoust. Soc. Am. 56: 1084-1091.

Duncan AJ, Gavrilov A and Li F, Acoustic propagation over limestone seabeds, Proceedings of ACOUSTICS 2009, 23 – 25 November 2009, Adelaide, Australia.

Finneran JJ and Jenkins AK, 2012, Criteria and thresholds for U.S. Navy acoustic and explosive effects analysis. San Diego, California.

Gerez D, Groenaas H, Larsen OP, Wolfstirn M and Padula M, 2015, Controlling air-gun output to optimize seismic content while reducing unnecessary high-frequency emissions: 85th Annual International Meeting, SEG, Expanded Abstracts, 154–158.

Gisiner RC, 2016, Sound and marine seismic surveys, Acoustics Today, Winter Edition, pp. 10-18.

Gundalf Designer, Revision Gundalf™ 8.1k, 8 Apr 2016, Oakwood Computing Associates, UK & Singapore, (https://www.gundalf.com/).

Hamilton EL, 1980, Geoacoustic modelling of the sea floor, J. Acoust. Soc. Am. 68: 1313:1340.

Jensen FB, Kuperman WA, Porter, MB and Schmidt H, 2011, Computational Ocean Acoustics, Springer-Verlag New York.

Li B and Hall MV, 2012, The loss mechanisms of plane-wave reflection from the seafloor with elastic characteristics, Proceedings of Acoustics 2012 – Fremantle, 21-23 November 2012, Fremantle, Australia.

Locarnini RA, Mishonov AV, Antonov JI, Boyer TP, Garcia HE, Baranova OK, Zweng MM, and Johnson DR, 2010, World Ocean Atlas 2009, Volume 1: Temperature. S. Levitus, Ed. NOAA Atlas NESDIS 68, U.S. Government Printing Office, Washington, D.C., 184 pp.

National Marine Fisheries Service (NMFS), 2016, Technical Guidance for Assessing the Effects of Anthropogenic Sound on Marine Mammal Hearing: Underwater Acoustic Thresholds for Onset of Permanent and Temporary Threshold Shifts. U.S. Dept. of Commer., NOAA. NOAA Technical Memorandum NMFS-OPR-55, 178 p.

Parkes GE and Hatton L, 1986, The Marine Seismic Source, 1st ed. Springer Science + Business Media, Dordrecht, The Netherlands, doi:10.1007/978-94-017-3385-4.Ziolkowski A, 1970, A method for calculating the output pressure waveform from an air-gun, Geophys. J. R. Astr. Soc., 21, pp. 137-161.

Porter M, 2010, Acoustics Toolbox in Ocean Acoustics Library (http://oalib.hlsresearch.com/).

Saunders PM and Fofonoff NP, 1976, Conversion of pressure to depth in the ocean, Deep-Sea Res. 23: 109-111.

Southall BL, Bowles AE, Ellison WT, Finneran J, Gentry R, Green CR, Kastak CR, Ketten DR, Miller JH, Nachtigall PE, Richardson WJ, Thomas JA and Tyack PL, 2007, Marine mammal noise exposure criteria. - Aquatic Mammals 33:411-521.

Teledyne Bolt Technology Corporation, 2017, Teledyne Products: Seismic Source Air Guns, (http://www.teledynemarine.com/air-guns), viewed 30 May 2017.

Teledyne Blog, Calmer waters: reducing sound exposure to marine mammals during seismic surveys, viewed 05 June 2017, (http://www.teledynemarine.com/blog/environmentally-conscious-energy-source), viewed 10 March 2017.